



**HAL**  
open science

# History dependent plasticity of glass: A mapping between atomistic and elasto-plastic models

David Castellanos, Stéphane Roux, Sylvain Patinet

► **To cite this version:**

David Castellanos, Stéphane Roux, Sylvain Patinet. History dependent plasticity of glass: A mapping between atomistic and elasto-plastic models. *Acta Materialia*, 2022, 241, pp.118405. 10.1016/j.actamat.2022.118405 . hal-03867525

**HAL Id: hal-03867525**

**<https://hal.science/hal-03867525>**

Submitted on 23 Nov 2022

**HAL** is a multi-disciplinary open access archive for the deposit and dissemination of scientific research documents, whether they are published or not. The documents may come from teaching and research institutions in France or abroad, or from public or private research centers.

L'archive ouverte pluridisciplinaire **HAL**, est destinée au dépôt et à la diffusion de documents scientifiques de niveau recherche, publiés ou non, émanant des établissements d'enseignement et de recherche français ou étrangers, des laboratoires publics ou privés.

# History dependent plasticity of glass: a mapping between atomistic and elasto-plastic models

David F. Castellanos<sup>a</sup>, Stéphane Roux<sup>b</sup>, Sylvain Patinet<sup>a,\*</sup>

<sup>a</sup>*PMMH, CNRS, ESPCI Paris, Université PSL, Sorbonne Université, Université de Paris, 75005 Paris, France*

<sup>b</sup>*Université Paris-Saclay, ENS Paris-Saclay, CNRS, LMPS - Laboratoire de Mécanique Paris-Saclay, F-91190, Gif-sur-Yvette, France*

---

## Abstract

Mesoscale elasto-plastic models, with statistically distributed structural properties and elastic coupling between discrete blocks, have been shown to quantitatively reproduce the main phenomenology observed in the *stationary flow state* of glasses as modelled at the atomic scale [1]. In the present study, an extension of such approaches is proposed to describe the transient mechanical response of glasses from different off-equilibrium states in the athermal quasi-static limit. Equilibrated liquids are simulated using two-dimensional molecular dynamics, quenched instantaneously to zero temperature, and then sheared. The mechanical observables measured in atomistic and elasto-plastic models are compared at the same length scales to calibrate a state-dependent constitutive law. A physical mechanism is proposed where the structural properties' evolution rate depends on the magnitude of local plastic deformation events, introducing an effective local memory of previous states in the system. This mechanism naturally leads to a brittle-ductile transition in the mechanical response of glasses, which depends exclusively on the quenched structure. Specifically, initially stable glasses exhibit strain-softening and localization, where the memory of the initial states is lost abruptly after the first plastic rearrangements. On the other hand, systems quenched from high-temperature liquids show a slow strain-hardening with statistically homogeneous plastic deformation. In these initially soft glasses, numerous plastic rearrangements are required to converge toward the stationary flow state. The elasto-plastic model successfully reproduces the stress-strain curves in the transient regime for the whole range of parent temperatures by including this local memory mechanism. The limitations of the model are finally discussed, together with possible improvements.

*Keywords:* Multi-scale modelling, Amorphous solids, Plasticity, Mesoscale, Atomistic, Yield threshold, Transient response, Off-equilibrium states

---

## 1. Introduction

Understanding the physical mechanisms that lead to the deformation of amorphous solids is still an ongoing fundamental problem [2, 3], with implications in engineering and microstructural designs [4, 5]. Amorphous solids, and specifically glasses, are out-of-equilibrium systems, implying a dependence on past thermal [6] and mechanical history [7]. Consequently, preparation protocols lead to highly contrasted mechanical responses depending on the degree of structural stability [8]. Glasses quenched from equilibrated states at low parent temperature exhibits a brittle-like behaviour, characterized by a stress-overshoot followed by strain-softening and permanent shear-banding. On the other hand, glasses obtained from high parent temperatures exhibit ductile-like behaviours characterized by a more compliant response, slow strain-hardening, and statistically homogeneous plastic activity.

In addition to history dependency [9], the complexity of their plastic behaviour arises from their microscopic disordered structures. Any coarse-grained description of amorphous plasticity has thus to deal with the statistical nature of their structures and their complex energy landscapes [10, 11, 12, 13]. Their properties are locally heterogeneous, and they feature prestresses, even in the reference state, before any plastic deformation [14]. In glassy systems, plasticity results from localized atomistic rearrangements known as shear transformations (STs) [15, 16] that give rise to long-range internal stress fields [17, 18]. Elastic coupling induced by the STs gives rise to intermittent deformation in the form of strain bursts [19]. To date, there are no physically motivated standard constitutive laws for amorphous media, in sharp contrast with crystal plasticity models where dislocation densities along local slip systems play the role of internal variables [20, 21, 22].

Numerous mesoscale elasto-plastic models of the plastic deformation of amorphous solids have been proposed in the literature over the last decades [23, 24, 25, 26, 27, 28, 29, 30] with the goal of shedding light on the physical mechanisms at play at the lowest scales. These models attempt to reduce the complexity of the prob-

---

<sup>\*</sup>Fully documented templates are available in the elsarticle package on CTAN.

<sup>\*</sup>Corresponding author

Email address: [sylvain.patinet@espci.fr](mailto:sylvain.patinet@espci.fr) (Sylvain Patinet)

lem by coarse-graining atomistic details into a discrete-continuum description. Spatially, STs are modelled as Eshelby inclusions [31, 32, 33, 34] with purely deviatoric eigenstrains. On the other hand, structural heterogeneity is accounted for by considering a statistically distributed local yield stress field [35]. Such models are well-known for reproducing the main features of the plastic deformation of amorphous solids in the stationary flow regime [36]. These models have also been successfully extended to address mechanical response at finite temperature, e.g., for creep [24, 37, 38, 39]. However, comparatively little attention has been given to the dependence upon initial quench states and to the transient regime [40, 41, 38, 42]. In addition, the ingredients of the models are most often phenomenological, and only a few works rely on microscopic insight from atomistic methods [43, 44, 45].

In this work, we take advantage of the two-dimensional tensorial elasto-plastic model developed in [1]. This model has shown quantitative agreement with atomistic simulations in the stationary flow regime. Thanks to its ability to deal with ST flow in different directions, it was shown to capture emergent phenomena such as the Bauschinger effect, i.e. deformation-induced anisotropy. This model is extended here by introducing a new constitutive relation that explicitly considers non-stationarity in the local structural renewal process. This relation accounts for the history-dependent mechanical response observed in the atomistic glasses. This framework introduces a simple and physically motivated memory effect at the local scales.

Both models are compared in the athermal quasi-static limit for a wide range of parent temperatures, establishing a rigorous connection between elasto-plastic and atomistic descriptions. These preparation protocols lead to highly contrasted mechanical responses, from soft to hard glasses, showing a progressive strain-hardening or a sudden strain-softening and localization, respectively. The frozen matrix method [35, 1] is employed to probe the local mechanical response of the atomistic and elasto-plastic samples at the same length scales. These measurements allow us to calibrate the elasto-plastic model in the quench states and transient regimes while keeping some elements of microscale physics, thus shedding light on history-dependent processes and the origins of the brittle-ductile transition.

The paper starts by introducing the atomistic system in Sec. 2 and the elasto-plastic model ingredients in Sec. 3. The frozen matrix methods to probe the local mechanical properties at different length scales in both models are then presented. The elasto-plastic model is enriched to deal with the local evolution of structural properties under plastic deformation. This model is then calibrated to reproduce the quench states obtained from a set of different parent temperatures. Sec. 4 deals with the transient mechanical response of glasses focusing on the characteristic strain needed to converge toward steady flow microscopic properties. The variation of shear modulus and strain localisation under imposed deformation are analysed. We finally discuss in Sec. 5 the discrepancies between the two

models and the insights gained from this multi-scale approach.

## 2. Atomistic model

We consider a two-dimensional binary model for generating and probing the mechanical response of glasses. Its plastic behaviour has been extensively studied in [46, 47, 7]. This model has been employed as a reference system for a systematic and quantitative calibration of an enriched elasto-plastic model in [1]. The simulations are performed with periodic boundary conditions for systems made of  $10^4$  atoms with number density  $\approx 1.02$ . The atoms interact through Lennard-Jones (LJ) interatomic potentials parametrized by their energy  $\epsilon$  and length  $\sigma$  scales. The mass  $m$  of each particle is unity, and the unit of time is  $\sigma\sqrt{m/\epsilon}$ . Boltzmann's constant is taken as unity, and the LJ units are used in the following. The LJ expression for an interatomic distance greater than  $R_{in} = 2$  is replaced by a quartic polynomial vanishing function at the cutoff distance  $R_{cut} = 2.5$ .

The glasses are obtained from instantaneous quenches of liquids at thermodynamic equilibrium simulated by molecular dynamics (MD) over a duration equal to 100 times the liquid relaxation times. A wide range of parent temperatures is studied from  $T_p = 0.32$  to  $0.7$ , ranging from the supercooled liquid regime to the simple liquid diffusion regime. This temperature range is chosen to overlap the mode coupling temperature  $T_{MCT} \approx 0.373$ [47] while still being able to achieve thermodynamic equilibrium with conventional MD, i.e. above of the computer glass transition temperature  $T_g \approx 0.31$ . After the quench, the glasses are relaxed by a conjugate gradient algorithm and then deformed in simple shear along the xy direction following the athermal quasi-static (AQS) method [19]. This procedure consists in applying small increments of affine deformation to the simulation box  $\Delta\gamma_{ext} = 10^{-4}$  followed by a static relaxation. Depending on initial states, the stationary flow state for this system under AQS can be reached for strains of the order of  $\gamma_{ext} \gtrsim 5$  [7]. Here we shall investigate only the transient regime and deform the resulting glasses to a total strain of  $\gamma_{ext} = 0.5$ . In addition to the plastic response, the overall system's elastic shear modulus  $G$  is computed as a function of  $\gamma_{ext}$ . The data reported in the article correspond to ensemble averages computed over 30 independent samples simulated for each preparation protocol.

As previously reported [6, 46, 8], the average mechanical response shown in figure Fig. 1 presents a marked dependence on the thermal history of the glass. The lower the equilibrium parent temperature, the stiffer and harder the glass. For the lowest  $T_p$ , the amorphous solid exhibits a stress-overshoot marking the start of strain-softening associated with the appearance of shear bands. On the other hand, glasses obtained from a high  $T_p$  are more compliant and exhibit a progressive slow hardening behaviour with a statistically homogeneous plastic deformation field.

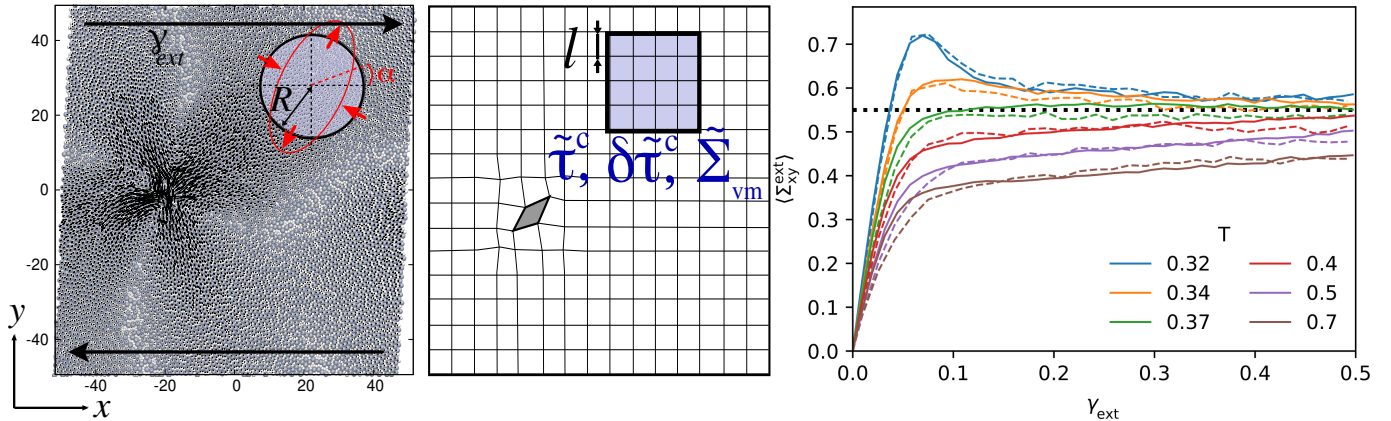


Figure 1: Left and middle: Atomistic and elasto-plastic models, respectively. The regular square grid is the mesh used in this work. The glass experiences a local shear transformation. The frozen matrix method is employed to probe the local mechanical response on different scales  $R$  (blue patches) and directions  $\alpha$ . Right: Global stress-strain curves under simple shear in the  $xy$  direction for atomistic (dashed lines) and elasto-plastic (continuous lines) models for glasses prepared from different parent temperatures  $T_p$ . The horizontal dotted line corresponds to the stationary flow stress.

In addition to the overall response, local yield stresses are computed with the frozen matrix method developed in [35, 46]. The method consists in deforming a patch of radius  $R$  (see the blue area in Fig. 1, left) following AQS pure shear boundary conditions. To this end, an affine pure shear in the direction  $\alpha$  is applied to the atoms of the surrounding matrix. Starting from the internal patch-scale shear stress  $\tilde{\tau}$ , the patch is loaded up to the onset of instability at the patch-scale yield stress  $\tilde{\tau}^c$ , from which the residual plastic strength (or equivalently the distance to threshold  $\Delta\tilde{\tau}^c = \tilde{\tau}^c - \tilde{\tau}$ ) is obtained. Following the instability, a ST occurs, leading to a stress drop  $\delta\tilde{\tau}^c$  within the patch. Patches are defined on a regular square grid of mesh parameter 2.5, every  $\Delta\alpha = 10^\circ$ , and for patch radii ranging from  $R = 2.5$  to 30.

### 3. Elasto-plastic model

The elasto-plastic model employed in this work is a direct extension of the one introduced in [1]. A continuum body discretized into a two-dimensional lattice of mesoscale elements is considered as depicted in Fig. 1, middle. Each element has a size  $l \times l$  where  $l$  is larger than the typical scale of a ST. Microscopic details below the element scale are not resolved. Consequently, the stress and strain fields are considered homogeneous within each element but can fluctuate over the material domain.

#### 3.1. Local slip systems

The amorphous microstructure is represented by considering that each mesoscale element contains several local slip systems with statistically distributed properties. The rationale behind using a discrete set of local slip planes per element is that STs can only occur in specific weak directions on a local scale, as shown in [46] from atomistic simulations. In the presence of strong structural disorder, planes that qualify as weak under the action of shear

stress may not qualify as such in other shear directions  $\alpha$ . While the slip system concept is more often used in the context of crystal plasticity to describe dislocation glide, it recently allowed us to reproduce the anisotropy induced by the plastic deformation in the same elasto-plastic framework [1].

Each local slip system is defined by a plane of normal unit vector  $\mathbf{n}$  and a slip direction  $\mathbf{s}$ , from which a Schmid tensor  $\mathbf{M} = \frac{1}{2}(\mathbf{s} \otimes \mathbf{n} + \mathbf{n} \otimes \mathbf{s})$  can be constructed. In two-dimension, this tensor can be written in terms of the angle  $\theta$  between the local slip plane and the horizontal axis as

$$\mathbf{M}(\theta) = \frac{1}{2} \begin{pmatrix} -\sin 2\theta & \cos 2\theta \\ \cos 2\theta & \sin 2\theta \end{pmatrix} \quad (3.1)$$

with  $\theta \in (-\pi/2, \pi/2]$  due to symmetry. The *resolved shear stress*  $\tau$  on a local slip plane is given by

$$\tau = \mathbf{M}(\theta) : \boldsymbol{\Sigma}, \quad (3.2)$$

where  $\boldsymbol{\Sigma}$  is the stress on the element. Each local slip system has a critical resolved shear stress, or slip threshold,  $\tau^c > 0$ . Whenever a local slip system fulfills  $\tau = \tau^c$ , it becomes *active* and a slip event takes place. This event aims at accounting, at the mesoscale, for the coarse-grained effects of a ST. To this end, a local (plastic) eigenstrain increment  $\Delta\boldsymbol{\varepsilon}_{\text{pl}}$  is added to the element in which the event takes place,

$$\Delta\boldsymbol{\varepsilon}_{\text{pl}} = \Delta\gamma_{\text{pl}}\mathbf{M}, \quad (3.3)$$

where the slip amplitude  $\Delta\gamma_{\text{pl}}$  along the local slip system is statistically distributed due to the (unresolved) microstructural heterogeneity. The following bounded power-law distribution is used

$$P(\Delta\gamma_{\text{pl}}|\gamma_{\text{max}}, \chi) = \frac{\chi}{\gamma_{\text{max}}} \left(1 - \frac{\Delta\gamma_{\text{pl}}}{\gamma_{\text{max}}}\right)^{\chi-1} \quad (3.4)$$

with  $\Delta\gamma_{\text{pl}} \in [0, \gamma_{\text{max}})$ . This form is chosen, as discussed in [1], since it allows to establish bounds to  $\Delta\gamma_{\text{pl}}$  while still allowing to tune its shape with a single parameter  $\chi$ .

To avoid negative dissipation [48], the parameter  $\gamma_{\max}$  writes

$$\gamma_{\max}(\tau) = \frac{-2\tau}{(\mathbb{C} : (\mathbb{S} - \mathbb{I}) : \mathbf{M}) : \mathbf{M}}, \quad (3.5)$$

and defines the plastic shear strain amplitude that would cancel a resolved shear stress  $\tau$ , assuming linear elasticity, where  $\mathbb{C}$  is the fourth-order Hooke's tensor, and  $\mathbb{S}$  is the Eshelby tensor of the mesoscale elements. In [1], the limit  $\gamma_{\max}(\tau)$  was used, meaning that the locally acting shear stress gives the amplitude of the events. In the present work, however, a limit  $\gamma_{\max}(\tau^c)$  based on the maximum shear stress  $\tau^c$  that a specific local slip plane can hold was found to reproduce better the transient flow regime, and hence this choice was adopted. After model calibration, both choices lead to similar results in the stationary regime.

The slip angles and thresholds are statistically distributed to represent structural heterogeneity. As discussed in [1], to ensure that elements have a finite critical resolved shear stress defined for any shear orientation  $\alpha$ ,  $N$  local slip systems, in groups of four, are introduced, with orientations  $\theta + n\pi/4$  where  $n = 1, 2, 3$  and  $4$ .  $\theta$  is uniformly distributed in the interval  $(-\pi/2, \pi/2]$ . The slip thresholds are independently renewed from the Weibull distribution

$$P(\tau^c|\lambda, k) = \frac{k}{\lambda} \left(\frac{\tau^c}{\lambda}\right)^{k-1} \exp\left[-\left(\frac{\tau^c}{\lambda}\right)^k\right], \quad (3.6)$$

where the parameter  $\lambda$  and the exponent  $k$  define the scale and the shape of the distribution, respectively. When an element undergoes a slip event, the orientations and thresholds of its  $N$  local slip systems are renewed from their respective probability distributions. This mechanism accounts for unresolved changes in the local microstructural properties induced by plastic deformation.

### 3.2. Dynamics

Whenever one or more local slip systems are active, slip events are simultaneously performed in all those systems. Influenced by stress redistribution, additional local slip systems might become active. The activation process is repeated in a series of steps until no local slip system is active. During this process, the external strain is kept fixed. If several local slip systems within the same mesoscale element are active simultaneously, only the local slip system with the lowest distance to threshold  $\Delta\tau^c = \tau^c - \tau$  undergoes a slip event. A quasi-static driving protocol is applied. To this end, whenever there is no active local slip system, discrete external shear strain increments are applied along the xy direction with the same amplitude  $\Delta\gamma_{\text{ext}} = 10^{-4}$  as in the atomistic model.

### 3.3. Computing the elastic fields

The Finite Element Method (FEM) is used to compute the displacement field at every time step, so that compatibility, balance, and constitutive relations are all obeyed.

[24, 49, 28, 50, 37, 38, 30]. A two-dimensional quadrilateral structured mesh of finite elements (FEs) is considered with linear shape functions. Each FE defines the spatial domain of a mesoscale element.

The total strain, *i.e.*, the symmetric part of the displacement gradient, is the sum of the elastic  $\boldsymbol{\varepsilon}_{\text{el}}$  and the plastic strain  $\boldsymbol{\varepsilon}_{\text{pl}}$ . The stress is related to the elastic strain through the linear elastic law  $\boldsymbol{\Sigma} = \mathbb{C} : \boldsymbol{\varepsilon}_{\text{el}}$ , where  $\mathbb{C}$  is the fourth-order Hooke's tensor, and the plastic strain  $\boldsymbol{\varepsilon}_{\text{pl}}$  is updated according to the model dynamics. The fields associated with each mesoscale element are naturally the coarse-grained average of the same quantity occurring at a smaller (microscopic) scale that cannot be resolved. Thus, we associate to each mesoscale element the average of each field computed over its associated FE.

Bi-periodic boundary conditions are used with an externally applied shear strain  $\gamma_{\text{ext}}$  along the xy direction. The external shear stress  $\Sigma_{\text{ext}}^{\text{xy}}$  is computed as the average shear stress over the system.

### 3.4. Transient properties

Atomistic measurements [35, 7] evidence that quenched state structural properties differ from the stationary state ones. In the elasto-plastic model, this difference is introduced by considering that the distribution parameters of the distribution Eq. 3.6 evolve as a function of local plastic deformation, thus spatially fluctuating. We consider a linear evolution law for parameter evolutions as a consequence of local plastic deformation. Thus, for the parameter  $\lambda$ ,

$$\Delta\lambda = (\partial\lambda/\partial\gamma_{\text{pl}})\Delta\gamma_{\text{pl}}, \quad (3.7)$$

and

$$(\partial\lambda/\partial\gamma_{\text{pl}}) = (\lambda_s - \lambda)/\gamma_t, \quad (3.8)$$

where  $\lambda_s$  is the stationary state value, and  $\gamma_t > 0$  is a characteristic plastic strain scale. This law can be interpreted as the dominant term (*i.e.*, with the largest relaxation strain  $\gamma_t$ ) in a small perturbation expansion of a possibly more complex law. If the scale  $\gamma_t$  is constant, Eq. 3.9 reduces to an exponential function of the local accumulated plastic strain.

Nonetheless, we consider a more general approach in which no constraints on  $\gamma_t$  are imposed, and the values of  $\lambda$  are updated based only on local changes  $\Delta\gamma_{\text{pl}}$  instead of on accumulated values. To this end, we first index the system history according to the number  $n$  of plastic events that have occurred so far. Thus, transition from  $n$  to  $n+1$  takes place due to a local plastic increment of amplitude  $\Delta\gamma_{\text{pl}}^{(n)}$ . We integrate Eq. 3.8 between the current state  $n$  and the next state  $n+1$ , and consider the limits  $\lambda \in [\lambda^{(n)}, \lambda^{(n+1)}]$  and  $\Delta\gamma_{\text{pl}} \in [0, \Delta\gamma_{\text{pl}}^{(n)}]$ , which result in the exponential form

$$\lambda^{(n+1)} = (\lambda^{(n)} - \lambda_s) \cdot \exp\left(-\frac{\Delta\gamma_{\text{pl}}^{(n)}}{\gamma_t}\right) + \lambda_s \quad (3.9)$$

For the sake of simplicity, an analogous form is considered for the shape parameter  $k$  of Eq. 3.6, with an asymptotic

value  $k_s$ . To keep the model formulation simple enough,  $\chi$  is assumed to be constant so that the plastic rearrangement amplitude relations (see Eq. 3.4 and Eq. 3.5) do not change with the deformation. The following limits hold,

$$\begin{aligned} \lambda^{(n+1)} &\rightarrow \lambda^{(n)} & \text{if } \Delta\gamma_{\text{pl}}^{(n)}/\gamma_t &\rightarrow 0 \\ \lambda^{(n+1)} &\rightarrow \lambda_s & \text{if } \Delta\gamma_{\text{pl}}^{(n)}/\gamma_t &\rightarrow \infty \end{aligned}$$

Thus, as intuitively expected, plastic events with a small plastic strain amplitude  $\Delta\gamma_{\text{pl}}$  result in renewed structural properties that remain statistically close to the previous ones. On the other hand, events with a larger amplitude result in a comparatively more significant change toward the asymptotic stationary value.

The model considers the evolution of the shear modulus  $G$  as a function of local plastic deformation. On the other hand, since the model is mainly sensitive to shear stresses, we make the simplifying assumption of a constant bulk modulus  $B$ , which is set to its stationary state value. We assume that the shear modulus  $G$  evolves locally according to a law with the same form as Eq. 3.9. Then, the model relies on an approximation for computational performance. Namely, the shear modulus is homogenized by replacing it with its spatial average. With the global values of  $G$  and  $B$ , a homogeneous and isotropic Hooke's tensor  $\mathbb{C}$  is created and used for computing the elastic fields as described in Sec. 3.3. Let us stress that the goal is to describe the effects of the variation of the elastic properties with strain only to the leading order. These homogeneous values will be compared to the effective atomistic ones measured at the sample scale in Fig. 6 below.

Finally, in order to implement recursive evolution laws with the form of Eq. 3.9, the initial values  $\lambda^{(1)}$ ,  $k^{(1)}$ , and  $G^{(1)}$  are needed. These values are respectively given by the quench state values  $\lambda_q$ ,  $k_q$ , and  $G_q$ , which correspond to model-free parameters to be fitted. On the other hand, the stationary state values  $\lambda_s$ ,  $k_s$  and  $G_s$  are known from [1].

## 4. Results

As explained in Sec. 2, atomistic glass samples are prepared with parent liquid temperatures of  $T_p = 0.32, 0.34, 0.37, 0.4, 0.5$  and  $0.7$ . The goal is to reproduce the atomistic quench state properties and the transient flow regime for the whole temperature range using the elasto-plastic model. To this end, the stationary state results of [1] are leveraged. The mesoscale element length is set to  $l = 6.6$  and the number of local slip systems per element to  $N = 36$ . For this model configuration, the optimum values for the stationary state parameters  $\lambda_s$ ,  $k_s$ ,  $\chi$ ,  $G_s$  and  $B_s$  are given in Tab. B.1. These values are independent of the initial conditions and thus of the parent temperature  $T_p$ .

### 4.1. Quenched state

The quenched shear modulus  $G_q$  is measured from the macroscale elastic response of atomistic glasses with different parent temperatures  $T_p$ . The bulk modulus is set to

its stationary state value  $B_s$ , independently of  $T_p$ . These values are used as input for the elasto-plastic model, considering isotropic and homogeneous elastic properties.

To calibrate the local properties, the frozen matrix method is employed as schematized in Fig. 1 (left and middle, blue areas). It allows us to compare the local mechanical response independently of model implementation details and at different length scales. The method is applied to the atomistic samples as described in Sec. 2. On the other hand, the implementation of the same method, presented in [1], is used for the elasto-plastic model. Local properties are calibrated by requiring that patch-scale values, when measured at the largest patch size available, are statistically similar between both models. In the case of the atomistic model, the largest patch has a radius of  $R = 30$ . As detailed in [1], this is compared with square elasto-plastic patches of the same area. For the chosen mesoscale length of  $l = 6.6$ , such patches are composed of  $8 \times 8 = 64$  mesoscale elements. Moreover, since the quenched state is statistically isotropic, aggregated measurements do not depend on the shear orientation  $\alpha$ . Thus, we compute aggregated quantities by pooling patch-scale data from local shear tests with different shear orientations.

To induce an internal stress field akin to the residual quenched stresses resulting from the atomistic sample preparation history and mimic the supercooled liquid relaxation process [51], a quenched eigenstrain plastic field  $\epsilon_{\text{pl}}^0$  is generated. We neglect the quenched state pressure field since the system dynamics are mostly sensitive to shear stresses. Thus,  $\epsilon_{\text{pl}}^0$  is assumed to be a purely deviatoric field. The two deviatoric components are (element-wise) independently drawn from a Gaussian distribution with zero average and standard deviation  $\text{std}[\text{dev}(\epsilon_{\text{pl}}^0)]$ . The standard deviation is calibrated by requiring that the patch-scale von Mises stress  $\tilde{\Sigma}_{\text{vm}}$  is statistically similar between both models. The process is repeated for each parent temperature  $T_p$  (see Fig. 2 top).

The initial slip configuration must be stable, given the stress field induced by  $\epsilon_{\text{pl}}^0$ . Thus, if an initial local slip system is active, all mesoscale element local slip systems are re-drawn from Eq. 3.6. This process is repeated until all local slip systems are stable, thus implementing a rejection sampling algorithm for constructing stable initial configurations.

The frozen matrix method is then applied to sample the patch-scale local yield stress values  $\tilde{\tau}^c$ . The individual slip thresholds, drawn from Eq. 3.6, and the measured coarse-grained yield stress  $\tilde{\tau}^c$  are observed to be different due to stress heterogeneity and patch-scale effects. The values of  $\lambda_q$  and  $k_q$  are calibrated by requiring statistically similar measurements of  $\tilde{\tau}^c$  in both models. The process is repeated for each parent temperature  $T_p$  as reported in Fig. 3 and Fig. 4.

As discussed in [46, 1, 45], small patches lead to an overestimation of  $\tilde{\tau}^c$  measurements in the atomistic model due to rigid boundary conditions (see Fig. 3 in the small

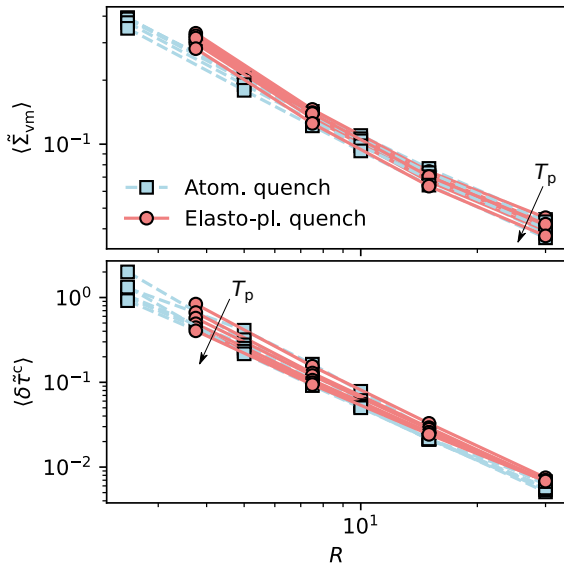


Figure 2: Average von Mises stress  $\langle \tilde{\Sigma}_{vm} \rangle$  (top) and stress drop  $\langle \delta \tilde{\tau}^c \rangle$  (bottom) vs. patch radius  $R$  for parent temperatures from  $T_p = 0.32$  to 0.7.

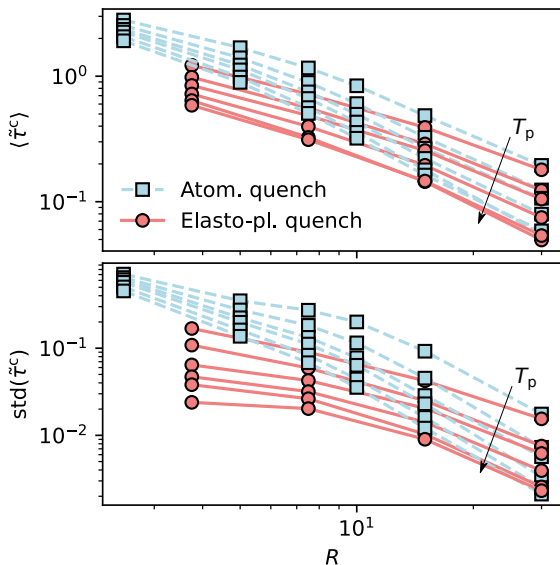


Figure 3: Average (top) and standard deviation (bottom) quench state local yield stress  $\tilde{\tau}^c$  vs. patch radius  $R$ , for parent temperatures from  $T_p = 0.32$ , to 0.7.

R range). For this reason, the comparison between models is performed with the largest patch size available. For this coarse length scale of  $R = 30$ , an excellent calibration is achieved in the quenched states for all the parent temperatures.

Regarding the patch-scale local stress drops  $\delta \tilde{\tau}^c$  induced by plastic deformation, we observe an excellent agreement between both models (see Fig. 2 bottom) once the local stress and yield thresholds have been calibrated.

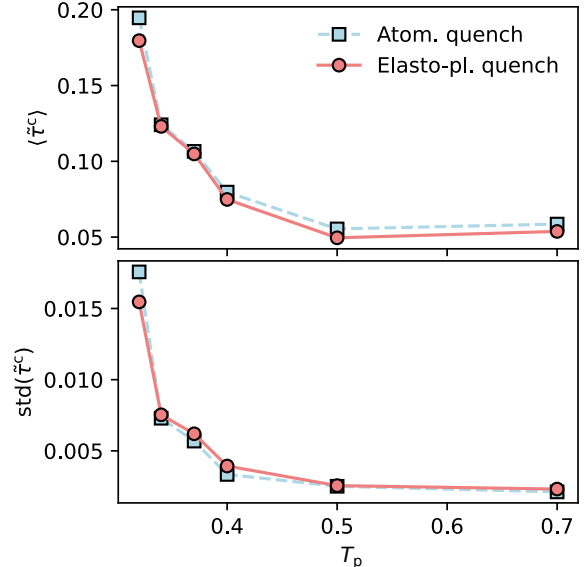


Figure 4: Average (top) and standard deviation (bottom) quench state local yield stress  $\tilde{\tau}^c$  vs. parent temperature  $T_p$ , measured with patch radius  $R = 30$ .

#### 4.2. Transient regime

With the quantitative calibration of the quench state discussed in Sec. 4.1 and the steady-state flow provided in [1], we focus now in the transient regime. It was suggested previously that the transient regime, and its memory effects, are ruled by Eq. 3.9. In principle, the value of  $\gamma_t$  is expected to be intrinsic to the athermal system dynamics and thus does not depend on parent temperature or initial conditions. In Fig. 5, different orders of characteristic strains  $\gamma_t$  are used, namely  $\gamma_t = 0.02, 0.2$ , and 2. The smallest  $\gamma_t = 0.02$  approaches the no-memory limit  $\gamma_t \rightarrow 0$ . For this value, the model reproduces the mechanical response of samples close to the mode coupling temperature  $T_{MCT}$ , since in this case, the properties of the quenched state are similar to the steady-state flow ones (disregarding polarization effects [7, 1]). However, it fails to generalize to other temperatures. Specifically, we observe too fast convergence toward the steady-state. This observation motivates using a non-vanishing characteristic strain  $\gamma_t$  and supports the modelling approach chosen for the transient regime.

On the other hand, both  $\gamma_t = 0.2$  and  $\gamma_t = 2$  show excellent agreements but their best fits correspond to different  $T_p$  ranges. We find that  $\gamma_t = 0.2$  reproduces almost quantitatively the stable glasses response obtained from the lowest parent temperatures. In particular, the model describes the stress peak and the subsequent strain-softening observed for  $T_p = 0.32$ . However, for  $\gamma_t = 2$ , the elasto-plastic model misses the stress overshoot with a much too slow strain-softening, as shown in Fig. 5 bottom. This result can be compared with previous works [47, 45] employing the same atomic model and glass stability ranges. In [47], a characteristic rearrangement plastic

strain of  $\varepsilon_{\text{pl}}^* \approx 0.054$  was estimated from the evolution of  $\bar{\tau}^c$  with a coarse-graining length of  $R = 5$ . Taking into account the factor 2 for a slip  $\gamma = 2\varepsilon$  and the length scale difference between the patch and the element area, one finds a corresponding strain scale  $2\varepsilon_{\text{pl}}^* \pi R^2 / l^2 \approx 0.195$ , in close agreement with  $\gamma_t = 0.2$ .

The interpretation of  $\gamma_t$  in the framework of the present elasto-plastic model is not straightforward because of the involved distributions of slip amplitudes in Eq. 3.4. Starting from the quench state, if one assumes constant  $\gamma_t$  and slip orientation, then  $\Delta\gamma_{\text{pl}}^{(n)}$  can be interpreted in Eq. 3.9 as an accumulated plastic strain. However, the model deals with randomly oriented local slip systems. The characteristic strain  $\gamma_t$  is thus expected to be an upper estimate of the local plastic strain necessary to converge to the steady-state. One can estimate the average slip amplitude of the first plastic rearrangement in the quenched state to assess the rapid relaxation toward a steady-state. A rough approximation of this first slip amplitude for  $T_p = 0.32$  is given at the element scale by the average  $\langle \delta\bar{\tau}^c \rangle / G_q \approx 0.06$  which is slightly smaller. This estimate is, however, closer if we consider the optimized  $\gamma_t \approx 0.1$  computed from Eq. 4.1 (see below). In any case, this result confirms that the renewal process in hard glasses takes place almost instantaneously, and stable amorphous solids locally forget their initial state after the very first plastic events.

In sharp contrast, the convergence toward steady-state found in atomistic simulations is much slower for the high parent temperatures, as shown in Fig. 5. In this case, the unstable glasses experience progressive hardening akin to mechanical annealing. A good match is found between the atomistic and elasto-plastic models for a value  $\gamma_t \approx 2$ , meaning that each element has to undergo many plastic rearrangements before reaching a  $\langle \Sigma_{\text{ext}}^{\text{xy}} \rangle$  value comparable to the steady-state plateau.

A critical parent temperature, featuring the quickest asymptotics between the fast strain-softening and slow strain-hardening regimes, is found in the vicinity of the mode coupling temperature [47], for  $0.37 < T_p < 0.4$ . As discussed above, the reason is that for the mode coupling temperature, the quench state properties are very close to the steady-state ones if we ignore plasticity-induced anisotropy [7, 1]. In this case, the transient regime vanishes, leading to a negligible parameter gap  $(\lambda - \lambda_s)$ , and thus an undeterminate value of the relaxation strain  $\gamma_t$ . In summary, the picture reported above suggests a dependency of the characteristic plastic strain  $\gamma_t$  on the parent temperature  $T_p$ . This finding is key to understanding the plasticity of glasses better. Since the systems evolve in athermal conditions, under the same loading protocol, and the compositions of all the glass samples are identical, differences in the dynamics must be necessarily linked to differences in local quench structural properties. Thus, to account for a dependency on structural properties, we generalize the memory model of Eq. 3.9 by considering a

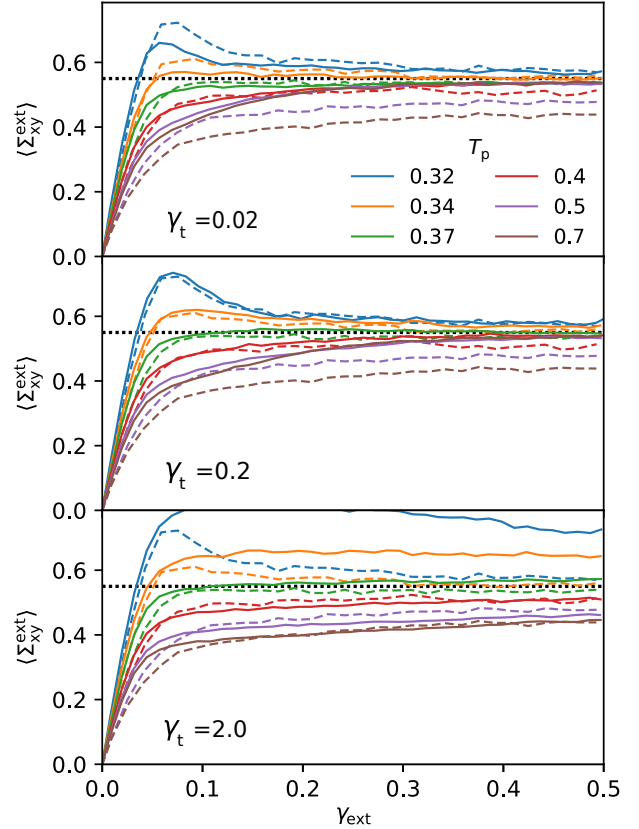


Figure 5: Stress-strain curves obtained with different fixed values of the  $\gamma_t$  parameter in Eq. 3.9. The continuous lines correspond to the elasto-plastic model and the dashed lines to the atomistic one. The dotted line is the steady-state value.

correction that depends on the local value of  $\lambda$  as

$$\gamma_t = \bar{\gamma}_t \left( \frac{\lambda^{(n)}}{\lambda_s} \right)^\beta \quad (4.1)$$

In this equation, the parameters  $\bar{\gamma}_t$  and  $\beta$  are intrinsic to the athermal system dynamics and do not depend on parent temperature or initial conditions. It means that  $\gamma_t$  now depends on  $(\lambda - \lambda_s)$ ; hence, we have lost the simple first-order character of Eq. 3.8, but still, everything is local during the structural evolution process.

For simplicity, the same correction based on  $\lambda$  is used for the other structural properties  $k$  and  $G$ . Strikingly, this corrected model allows for a rather accurate quantitative agreement in the stress-strain response, but this time over the whole temperature range as reported in Fig. 1 with  $\bar{\gamma}_t = 0.2$  and  $\beta = -3.3$ . Additional comparisons between the elasto-plastic model with the enriched relation Eq. 4.1 and the atomistic model are provided in Sec. Appendix A. Details of the fitting procedure and the estimated parameters are given in Sec. Appendix B.

#### 4.3. Evolution of elastic modulus

Plastic deformation is known to induce changes not only in the local yield stresses but also in the elastic mod-

uli [33] as a consequence of structural rejuvenation. As discussed in Sec. 3.4, the model considers the local evolution of the shear modulus with plastic deformation, assuming an evolution law first similar to Eq. 3.9, and then corrected by Eq. 4.1. However, elastic fields were computed for computational efficiency by considering only an average homogeneous  $G$ . To further check the consistency of the proposed approach, we compute these average shear moduli and compare them with the effective ones computed in atomistic simulation as a function of strain. To in-

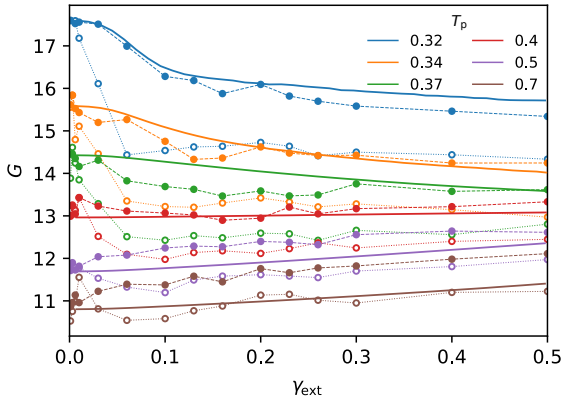


Figure 6: Global effective shear modulus vs. applied strain for different parent temperatures  $T_p$ , obtained from the elasto-plastic model (continuous lines), and the atomistic model in loaded states (open circles, dotted lines) and in unloaded states (full circles, dashed lines).

vestigate elastic nonlinearities, the shear moduli are measured in the atomistic simulations in the loaded and the unloaded states, as shown in Fig. 6. The unloading is carried out quasi-statically down to zero macroscopic shear stress. The unloading generates little plastic activity in agreement with [7]. This procedure, therefore, allows us to separate elastic nonlinearities from the effect of structural rejuvenation induced by plasticity.

Changes in modulus in the loaded state show a rapid drop in stiffness, especially at large external stresses, in stable glasses that feature a stress overshoot. This rapid drop is absent from the data in the unloaded state, which leads to the conclusion that it is mainly due to the increased external stress and, thence, elastic nonlinearities. The variation of the modulus of structural origin in the elasto-plastic model is described from the threshold evolution equations by replacing  $\lambda$  with  $G$  in Eq. 3.9 and Eq. 4.1. The comparison is made between the atomic simulations in the unloaded state and the calibrated elasto-plastic model in Fig. 6.

Although the evolution of the shear modulus was not part of the model calibration, this simplified modelling approach for the evolution of elastic properties can qualitatively reproduce the variations in the effective shear modulus obtained from atomistic simulations. Nevertheless, in agreement with [45], we note that the average macroscopic stress response is nearly unaffected if we neglect the global

elastic property variations.

#### 4.4. Local strain fluctuation

In addition to stress response, the mesoscopic model consistency is evaluated by analyzing the strain fields, which strongly depend on the thermal history of the glasses. For this, the local strain tensor  $\varepsilon$  is calculated from the deformation gradient tensor  $\mathbf{F}$ . For the elasto-plastic model,  $\mathbf{F}$  is numerically integrated for each element by multiplying the tensors  $\mathbf{F} = \mathbf{F}_n \mathbf{F}_{n-1} \cdots \mathbf{F}_2 \mathbf{F}_1$  where  $\mathbf{F}_i$  is the deformation gradient tensor between the states  $i$  and  $i + 1$  separating each plastic event.

For the atomistic simulations,  $\mathbf{F}$  is computed from the Zimmerman's approach [52] defining the atomic level deformation gradient tensor  $F_{ij}^\alpha$  for the atom  $\alpha$  from the (least square) minimization of the function

$$B^\alpha = \sum_{\beta=1}^n \sum_{i=1}^2 (x_i^{\alpha\beta} - F_{ij}^\alpha X_j^{\alpha\beta})^2, \quad (4.2)$$

where the sum is performed over the  $n$  nearest neighbours of  $\alpha$  located at a distance less than  $R_{CG}$  with  $\mathbf{X}^{\alpha\beta}$  and  $\mathbf{x}^{\alpha\beta}$  the distances between the atoms  $\alpha$  and  $\beta$  in the reference (the quench state here) and current configurations, respectively.

To quantitatively compare the local deformations of the two models, the strains are calculated on a length scale corresponding to the size of the elements of the elastoplastic model  $l$ . We employ a length  $R_{CG} = l/\sqrt{\pi}$  so that the considered area is the same for the atomistic coarse-grained strains and the mesoscopic elements. In addition,  $\mathbf{F}$  are spatially sampled on the same regular grid as the elasto-plastic model (see the mesh reported in Fig. 1) by assigning to each grid point the atomic value  $F_{ij}^\alpha$  corresponding to its nearest atom. The linear strain tensor  $\varepsilon$  is then calculated from  $\mathbf{F}$  and finally reduced to a scalar by considering the second invariant of the strain tensor  $\varepsilon_{VM}$ . Local strain maps are shown in Fig. 7(top) for the most contrasting parent temperatures,  $T_p = 0.32$  and  $0.7$ , in order to highlight the dependence of plastic strain fluctuations with the system's initial preparation. The strain fields calculated from the atomistic simulations (AT) and the elastoplastic model (EP) are illustrated for three imposed macroscopic strains equal to  $\gamma_{ext} = 0.15, 0.3$  and  $0.45$ .

The elasto-plastic model reproduces with a remarkable agreement the overall strain patterns observed in the atomistic model. For low parent temperatures, the strain field concentrates in the form of shear bands nucleated just after the stress peak, with a surrounding matrix almost not plastically deformed. Thereafter, the band widens with the increase in imposed deformation. While small fluctuations are still present in systems prepared from a high parent temperature, these soft glasses show statistically homogeneous plastic strain. The elasto-plastic model, therefore, consistently captures the ductile-fragile transition with the system preparation.

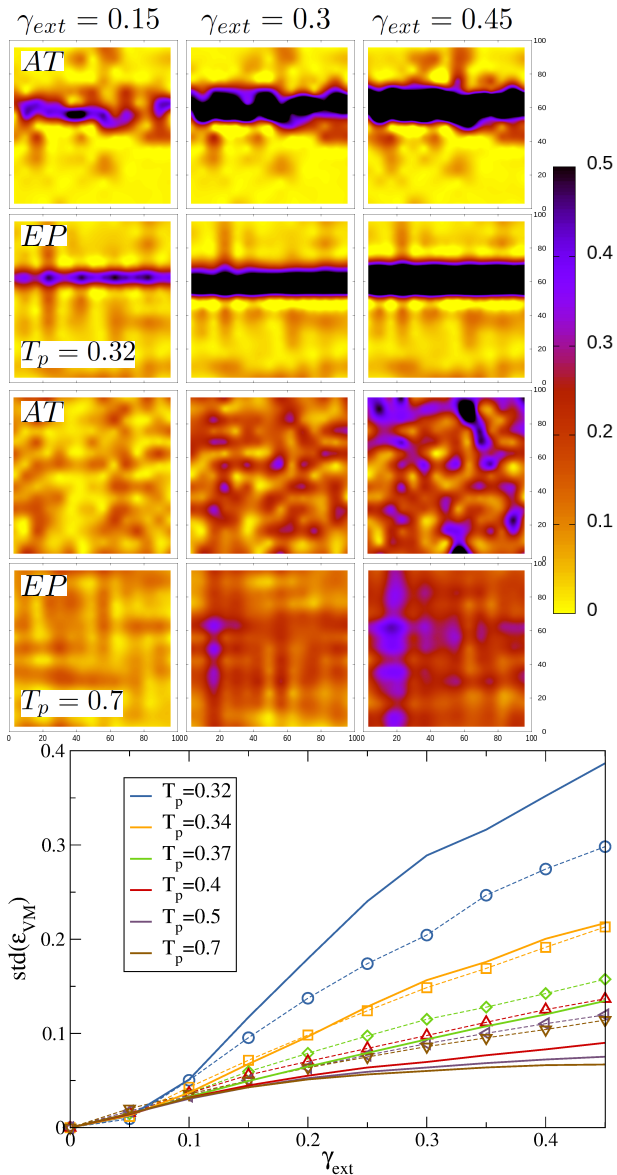


Figure 7: Top: local von Mises strain  $\varepsilon_{VM}$  maps for different applied deformations  $\gamma_{ext}$  (columns) and parent temperatures  $T_p$  (rows) computed from atomistic simulations (AT) and the elastoplastic model (EP). Bottom:  $\varepsilon_{VM}$  standard deviation as a function of  $\gamma_{ext}$  for different  $T_p$  obtained from the elasto-plastic model (continuous lines) and the atomistic model (open circles, dashed lines).

However, closer inspection of the strain fields computed in the mesoscopic model shows discrepancies with respect to the atomistic simulations. We indeed observe that the profile of the shear bands is less rough in the model, which features straighter bands. Similarly, the elastoplastic model for the high parent temperatures shows spatial correlations organising themselves into quasilinear patterns aligned with the mesh. We attribute part of this behaviour to the presence of soft modes in the elastic propagator as shown in [53].

To quantitatively compare the strain fluctuations of the two models, we report in Fig. 7(bottom) the strain standard deviation  $std(\varepsilon_{VM})$  as a function of  $\gamma_{ext}$ . As ex-

pected, we observe an increase in  $std(\varepsilon_{VM})$  with the applied strain and a decrease in the parent temperature. If the elasto-plastic model reproduces these trends qualitatively, it underestimates (overestimates) the fluctuations for high (low) parent temperatures. For the lowest  $T_p$ , the difference can be explained in particular by a slower spreading of the shear band with  $\gamma_{ext}$  and by the plastic event scarcity outside the band with respect to the atomistic simulations. In the case of soft glasses, the underestimation of  $std(\varepsilon_{VM})$  can be explained by the presence of large amplitude localised plastic rearrangements. Nevertheless, an excellent agreement is found around the ductile-brittle transition parent temperature for  $T_p = 0.34$ . Bearing in mind that the local strain fluctuations were not part of the adjustment, the model calibration thus appears here as a compromise that calls for considering other physical ingredients as discussed in the next section.

## 5. Discussion

We have shown that the extended elasto-plastic model can quantitatively match the macroscale mechanical response in the transient regime. This match is especially true for small  $T_p$ , which display a softening behaviour well captured by the calibration. Specifically, stable glasses are characterized by a memory of their quenched state much shorter than in unstable glasses quenched from relatively higher temperatures. Locally, this behaviour can be understood considering that glasses equilibrated at low  $T_p$  tend to have higher yield stresses, but as soon as refreshed by a plastic slip, the stable packing is almost entirely reshuffled and becomes, on average, softer. On a global scale, the observable softening behaviour is caused by the rapid localization of the deformation into a shear band. Shear bands are characterized by their softness compared to the surrounding matrix [47], which again supports a short memory. In contrast, for large  $T_p$ , the unstable glasses are "slow learners". In this case, it is difficult to reproduce a long memory in this elasto-plastic framework because the entire element is renewed. Hence, the model might compensate for excessive structural renewal with an increased apparent memory given by a larger value of  $\gamma_t$ . If we exclude the independent quench and steady-state calibrations, only the two parameters of the extended model given by Eq. 4.1 are required to match all the glass preparation protocols consistently.

While the physical interpretation of the  $\gamma_t$  value was discussed in Sec. 4.2, another question lies in the consistency of the calibrated exponents  $k$  reported in Tab. B.1 and B.2. In the limit  $\Delta\tau^c \rightarrow 0$ , a scaling law  $p(\Delta\tau^c) \propto (\Delta\tau^c)^\theta$  is indeed expected, but with a significantly smaller pseudogap exponent  $\theta$  (in the range 0.5 – 0.7 [46, 54]). The exponent  $k - 1$  (to compare with  $\theta$ ) however correspond to the  $\tau^c$  renewal distributions and not to  $\Delta\tau^c$ . Once decorated from internal stresses, we recover probability distribution functions for  $\Delta\tau^c$  in the steady state with an exponent  $\theta \approx 0.6$ , in excellent agreement with the literature results [55] (with

a plateau at low  $\Delta\tau^c$  due to finite size effects [56, 57]). For the quench states, the scaling is nevertheless less convincing. We ascribe this discrepancy to the caricaturally simple procedure employed to mimic the quench states, which only requires mechanical equilibrium and ignores the stress correlations observed in the inherent states [14]. Note that if atomistic simulations have shown that  $\theta$  is almost independent of the quench state [58, 59, 60], this is not the case for elasto-plastic models for which the question of a relevant preparation protocol remains open. The approaches developed in our work provide a first step to answering this.

As for the strain fluctuations discussed in Sec. 4.4, some small discrepancies regarding the stress response between the elasto-plastic and atomistic models should also be pointed out. First, Fig. 1 shows that the elasto-plastic model predicts slightly larger stresses than atomistic simulations in the pseudo-elastic regime at small applied strains for unstable glasses produced from high parent temperatures. Second, stress fluctuations are slightly overestimated as shown in Fig. A.8 for stable glasses. The origin of these two discrepancies can be presumably traced back to the statistics of plastic rearrangement amplitudes. For high  $T_p$ , the slip amplitudes are underestimated in the pseudo-elastic regime, slightly overestimating the stress response.

On the other hand, part of the overestimation of the fluctuation in the low  $T_p$  glasses comes from the constant coupling relationship between local thresholds and stress drops. These amplitudes are controlled by Eq. 3.4, supposedly independent of plastic strain in contrast to yield stress renewal distributions, which links structure relaxation through its dependence on the overcome slip thresholds. However, at the small scales at which slip events occur, elastic heterogeneity becomes relevant [61, 62]. Thus, a more accurate description of a slip event would explicitly consider the effects of local elastic heterogeneity as part of the event. Locally evolving elastic properties might also impact the event amplitude and the statistics of slip orientations.

The small strain regime may also suffer from the independent set of stresses and local slip systems during the quench state calibration, which neglects possibly more complex correlations beyond those introduced by the stability requirement discussed in Sec. 4.1. The effect of such a naive preparation protocol is presumably more significant in the case of high parent temperature glasses, where yield stresses are lower than for low  $T_p$  glasses. A modelling approach able to reproduce quenched states by explicitly incorporating the physics of the parent liquid state might thus be a way to improve the small strain responses [51]. Moreover, the observed discrepancies might be linked to some simplifying modelling assumptions, such as the postulated linearity, the neglect of finite deformation/rotation effects, the use of highly structured mesh, or the lack of convection [63] as discussed at length in [1].

## 6. Conclusions

In this paper, we have extended the description of the mechanical response of an elasto-plastic model of amorphous solids to the transient regime and for a wide range of initial system stabilities. The calibration of the model reproduces the different quench states obtained from the local atomistic data. A statistical model of the evolution of slip thresholds based on local plastic strain increments is proposed. This model shows an excellent agreement with atomistic simulations and makes it possible to reproduce the transient mechanical responses of glasses.

In stable glasses, showing a stress peak followed by strain-softening and localization, the transition to the stationary state is extremely rapid and occurs from the first plastic rearrangements. Conversely, the unstable glasses, quenched from high temperatures, require a much larger plastic strain and slowly harden towards the steady state. However, we show that to match the full range of behaviours within a unified model, it is necessary to explicitly consider the effects of the initial structure in the system's memory. With this correction, the model reproduces the transient responses with good precision for all the parent temperatures.

In total, *two* parameters are used to capture the instantaneous mechanical state ( $k$  and  $\lambda$ ), and a *third* parameter ( $\gamma_t$ ) is introduced to describe their evolution along shear. In this respect, the main message of our work is not the parameter fitting procedure but the fact that with only three parameters, it is possible to account precisely for the mean behaviour, its transient evolution from different initial states and its fluctuation in a continuous setting.

Future improvements should be considered regarding the consistent match between atomistic and elasto-plastic models. First, in the elastoplastic model, one could deal explicitly with elastic heterogeneity and anisotropy, which are known to become dominant at small scales [61, 62]. Another point would consist in assessing the effects of a constant FEM mesh. It is indeed expected that the ST size and density depend on thermomechanical history [64]. In this respect, the usage of non-uniform [50, 29] and history-dependent discretization would be of interest to explore the limit under which the continuous approach breaks down. As shown here and in previous studies [1, 45], the frozen matrix method seems to overestimate the measurements of the threshold values in atomistic simulations because of rigid boundary conditions. Another avenue would therefore consist in taking into account the deformation of the surrounding matrix, for instance, by resorting to flexible and elastic boundary conditions developed initially for dislocations [65]. All these enrichments are related to small-scale responses. As such, they could serve not only for more quantitative multi-scale approaches but also as a guide for a fundamental understanding of amorphous plasticity.

Several perspectives can be drawn from the present study for larger and continuous scales. To leverage the

computational efficiency of elasto-plastic models, homogenization techniques and coarser descriptions are logical next steps. Here, we have assumed that any deformation completely renews the local slip systems configuration within a deforming element. However, this is true only if the discretization length  $l$  is close to or below the ST size. In general, for larger  $l$ , the structure of a portion of the element is expected to remain unaltered. The non-renewed portion leads to a scale-dependent memory term, which could be translated to evolution laws with the same procedure as in this work, but with a  $\gamma_t$  appropriately weighted by the relative size of the non-renewed structure relative to the element size. Another avenue would be to study the relevant statistical fluctuations retained during a coarse-graining procedure. A goal could be to transfer the knowledge acquired from mesoscale elasto-plastic approaches to existing engineering codes for submicron scale applications, where large plastic fluctuations and intermittency cannot be ignored. Finally, the presented approach could be straightforwardly generalized to other amorphous materials, such as covalent glasses or granular media, potentially enriching our understanding of the similarities (or lack of) between these materials regarding plastic activity and structural evolution. The mechanical response for three-dimensional systems [66] and at finite temperature could also be considered. In principle, these developments do not pose a problem, allowing this method to be generalized to more realistic systems.

## Acknowledgements

The L<sup>a</sup>T<sub>E</sub>X L<sup>a</sup>SIPS is gratefully acknowledged for its support under grant 20LL2000-129.

## References

- [1] D. F. Castellanos, S. Roux, S. Patinet, Insights from the quantitative calibration of an elasto-plastic model from a Lennard-Jones atomic glass, *Comptes Rendus. Physique* 22 (S3) (2021) 135–162. doi:10.5802/crphys.48.
- [2] D. Rodney, A. Tanguy, D. Vandembroucq, Modeling the mechanics of amorphous solids at different length scale and time scale, *Modelling and Simulation in Materials Science and Engineering* (8) (2011) 083001. doi:10.1088/0965-0393/19/8/083001.
- [3] D. Bonn, M. M. Denn, L. Berthier, T. Divoux, S. Manneville, Yield stress materials in soft condensed matter, *Rev. Mod. Phys.* 89 (2017) 035005. doi:10.1103/RevModPhys.89.035005.
- [4] D. L. McDowell, Simulation-assisted materials design for the concurrent design of materials and products, *JOM* 59 (9) (2007) 21. doi:10.1007/s11837-007-0111-7.
- [5] E. van der Giessen, P. A. Schultz, N. Bertin, V. V. Bulatov, W. Cai, G. Csányi, S. M. Foiles, M. G. D. Geers, C. González, M. Hütter, W. K. Kim, D. M. Kochmann, J. Llorca, A. E. Mattsson, J. Rottler, A. Shluger, R. B. Sills, I. Steinbach, A. Strachan, E. B. Tadmor, Roadmap on multiscale materials modeling, *Modelling and Simulation in Materials Science and Engineering* 28 (4) (2020) 043001. doi:10.1088/1361-651x/ab7150.
- [6] Y. Shi, M. L. Falk, Strain localization and percolation of stable structure in amorphous solids, *Phys. Rev. Lett.* 95 (2005) 095502. doi:10.1103/PhysRevLett.95.095502.
- [7] S. Patinet, A. Barbot, M. Lerbinger, D. Vandembroucq, A. Lemaître, Origin of the bauschinger effect in amorphous solids, *Phys. Rev. Lett.* 124 (2020) 205503. doi:10.1103/PhysRevLett.124.205503.
- [8] M. Ozawa, L. Berthier, G. Biroli, A. Rosso, G. Tarjus, Random critical point separates brittle and ductile yielding transitions in amorphous materials, *Proceedings of the National Academy of Sciences* 115 (26) (2018) 6656. doi:10.1073/pnas.1806156115.
- [9] N. C. Keim, J. D. Paulsen, Z. Zeravcic, S. Sastry, S. R. Nagel, Memory formation in matter, *Rev. Mod. Phys.* 91 (2019) 035002. doi:10.1103/RevModPhys.91.035002.
- [10] D. Rodney, C. Schuh, Distribution of thermally activated plastic events in a flowing glass, *Phys. Rev. Lett.* 102 (2009) 235503. doi:10.1103/PhysRevLett.102.235503.
- [11] D. Rodney, C. Schuh, Yield stress in metallic glasses: The jamming-unjamming transition studied through Monte Carlo simulations based on the activation-relaxation technique, *Physical Review B* 80 (18) (2009). doi:10.1103/PhysRevB.80.184203.
- [12] P. Cao, M. P. Short, S. Yip, Potential energy landscape activations governing plastic flows in glass rheology, *Proceedings of the National Academy of Sciences* 116 (38) (2019) 18790. doi:10.1073/pnas.1907317116.
- [13] B. Xu, M. L. Falk, S. Patinet, P. Guan, Atomic nonaffinity as a predictor of plasticity in amorphous solids, *Phys. Rev. Materials* 5 (2021) 025603. doi:10.1103/PhysRevMaterials.5.025603.
- [14] A. Lemaître, Structural relaxation is a scale-free process, *Phys. Rev. Lett.* 113 (2014) 245702. doi:10.1103/PhysRevLett.113.245702.
- [15] A. Argon, Plastic deformation in metallic glasses, *Acta Metallurgica* 27 (1) (1979) 47. doi:10.1016/0001-6160(79)90055-5.
- [16] M. L. Falk, J. S. Langer, Dynamics of viscoplastic deformation in amorphous solids, *Phys. Rev. E* 57 (6) (1998) 7192.
- [17] A. Tanguy, F. Leonforte, J.-L. Barrat, Plastic response of a 2d lennard-jones amorphous solid: Detailed analysis of the local rearrangements at very slow strain rate, *The European Physical Journal E* 20 (3) (2006) 355. doi:10.1140/epje/i2006-10024-2.
- [18] K. W. Desmond, E. R. Weeks, Measurement of stress redistribution in flowing emulsions, *Phys. Rev. Lett.* 115 (2015) 098302. doi:10.1103/PhysRevLett.115.098302.
- [19] C. Maloney, A. Lemaître, Subextensive scaling in the athermal, quasistatic limit of amorphous matter in plastic shear flow, *Phys. Rev. Lett.* 93 (2004) 016001. doi:10.1103/PhysRevLett.93.016001.
- [20] A. M. Cuitino, M. Ortiz, Computational modelling of single crystals, *Modelling and Simulation in Materials Science and Engineering* 1 (3) (1993) 225. doi:10.1088/0965-0393/1/3/001.
- [21] L. Tabourot, M. Fivel, E. Rauch, Generalised constitutive laws for f.c.c. single crystals, *Materials Science and Engineering: A* 234-236 (1997) 639. doi:https://doi.org/10.1016/S0921-5093(97)00353-5.
- [22] Y. Estrin, L. Tóth, A. Molinari, Y. Bréchet, A dislocation-based model for all hardening stages in large strain deformation, *Acta Materialia* 46 (15) (1998) 5509. doi:https://doi.org/10.1016/S1359-6454(98)00196-7.
- [23] V. V. Bulatov, A. S. Argon, A stochastic model for continuum elasto-plastic behavior. i. numerical approach and strain localization, *Modelling and Simulation in Materials Science and Engineering* 2 (2) (1994) 167. doi:10.1088/0965-0393/2/2/001.
- [24] E. R. Homer, C. A. Schuh, Mesoscale modeling of amorphous metals by shear transformation zone dynamics, *Acta Materialia* 57 (9) (2009) 2823. doi:10.1016/j.actamat.2009.02.035.
- [25] E. A. Jagla, Shear band dynamics from a mesoscopic modeling of plasticity, *Journal of Statistical Mechanics: Theory and Experiment* 2010 (12) (2010) 12025. doi:10.1088/1742-5468/2010/12/P12025.
- [26] M. Talamali, V. Petäjä, D. Vandembroucq, S. Roux, Strain localization and anisotropic correlations in a mesoscopic model of amorphous plasticity, *Comptes Rendus Mécanique* 340 (4–5) (2012) 275, recent *Advances in Micromechanics of Materials*.

- doi:<http://dx.doi.org/10.1016/j.crme.2012.02.010>.
- [27] C. Liu, E. E. Ferrero, F. Puosi, J.-L. Barrat, K. Martens, Driving rate dependence of avalanche statistics and shapes at the yielding transition, *Phys. Rev. Lett.* 116 (2016) 065501. doi:10.1103/PhysRevLett.116.065501.
- [28] Z. Budrikis, D. F. Castellanos, S. Sandfeld, M. Zaiser, S. Zapperi, Universal features of amorphous plasticity, *Nature Communications* 8 (2017) 15928.
- [29] K. Karimi, E. E. Ferrero, J.-L. Barrat, Inertia and universality of avalanche statistics: The case of slowly deformed amorphous solids, *Physical Review E* 95 (1) (2017) 013003. doi:10.1103/PhysRevE.95.013003.
- [30] F. Van Loock, L. Brassart, T. Pardoen, Implementation and calibration of a mesoscale model for amorphous plasticity based on shear transformation dynamics, *International Journal of Plasticity* 145 (2021) 103079.
- [31] J. D. Eshelby, The determination of the elastic field of an ellipsoidal inclusion, and related problems, *Proceedings of the Royal Society of London. Series A, Mathematical and Physical Sciences* 241 (1226) (1957) 376.
- [32] F. Puosi, J. Rottler, J.-L. Barrat, Time-dependent elastic response to a local shear transformation in amorphous solids, *Phys. Rev. E* 89 (2014) 042302. doi:10.1103/PhysRevE.89.042302.
- [33] T. Albaret, A. Tanguy, F. Boioli, D. Rodney, Mapping between atomistic simulations and eshelby inclusions in the shear deformation of an amorphous silicon model, *Phys. Rev. E* 93 (2016) 053002. doi:10.1103/PhysRevE.93.053002.
- [34] F. Boioli, T. Albaret, D. Rodney, Shear transformation distribution and activation in glasses at the atomic scale, *Phys. Rev. E* 95 (2017) 033005. doi:10.1103/PhysRevE.95.033005.
- [35] S. Patinet, D. Vandembroucq, M. L. Falk, Connecting local yield stresses with plastic activity in amorphous solids, *Phys. Rev. Lett.* 117 (2016) 045501. doi:10.1103/PhysRevLett.117.045501.
- [36] A. Nicolas, E. E. Ferrero, K. Martens, J.-L. Barrat, Deformation and flow of amorphous solids: Insights from elastoplastic models, *Reviews of Modern Physics* 90 (4) (2018) 045006. doi:10.1103/RevModPhys.90.045006.
- [37] D. F. Castellanos, M. Zaiser, Avalanche behavior in creep failure of disordered materials, *Phys. Rev. Lett.* 121 (2018) 125501. doi:10.1103/PhysRevLett.121.125501.
- [38] D. F. Castellanos, M. Zaiser, Statistical dynamics of early creep stages in disordered materials, *The European Physical Journal B* 92 (7) (2019) 139. doi:10.1140/epjb/e2019-100124-0.
- [39] M. Popović, T. W. J. de Geus, W. Ji, A. Rosso, M. Wyart, Scaling description of creep flow in amorphous solids (2021). arXiv:2111.04061.
- [40] D. Tüszes, P. Ispanovity, M. Zaiser, Disorder is good for you: The influence of local disorder on strain localization and ductility of strain softening materials, *International Journal of Fracture* 205 (2017) 139.
- [41] M. Popović, T. W. J. de Geus, M. Wyart, Elastoplastic description of sudden failure in athermal amorphous materials during quasistatic loading, *Phys. Rev. E* 98 (2018) 040901. doi:10.1103/PhysRevE.98.040901.
- [42] H. J. Barlow, J. O. Cochran, S. M. Fielding, Ductile and brittle yielding in thermal and athermal amorphous materials, *Phys. Rev. Lett.* 125 (2020) 168003. doi:10.1103/PhysRevLett.125.168003.
- [43] F. Puosi, J. Olivier, K. Martens, Probing relevant ingredients in mean-field approaches for the athermal rheology of yield stress materials, *Soft Matter* 11 (38) (2015) 7639. doi:10.1039/C5SM01694K.
- [44] A. R. Hinkle, C. H. Rycroft, M. D. Shields, M. L. Falk, Coarse graining atomistic simulations of plastically deforming amorphous solids, *Physical Review E* 95 (5) (2017) 053001. doi:10.1103/PhysRevE.95.053001.
- [45] C. Liu, S. Dutta, P. Chaudhuri, K. Martens, Elastoplastic approach based on microscopic insights for the steady state and transient dynamics of sheared disordered solids, *Phys. Rev. Lett.* 126 (2021) 138005. doi:10.1103/PhysRevLett.126.138005.
- [46] A. Barbot, M. Lerbinger, A. Hernandez-Garcia, R. García-García, M. L. Falk, D. Vandembroucq, S. Patinet, Local yield stress statistics in model amorphous solids, *Phys. Rev. E* 97 (2018) 033001. doi:10.1103/PhysRevE.97.033001.
- [47] A. Barbot, M. Lerbinger, A. Lemaître, D. Vandembroucq, S. Patinet, Rejuvenation and shear banding in model amorphous solids, *Phys. Rev. E* 101 (2020) 033001. doi:10.1103/PhysRevE.101.033001.
- [48] M. Vasoya, B. Kondori, A. A. Benzerga, A. Needleman, Energy dissipation rate and kinetic relations for eshelby transformations, *Journal of the Mechanics and Physics of Solids* 136 (2020) 103699, the Davide Bigoni 60th Anniversary Issue. doi:10.1016/j.jmps.2019.103699.
- [49] S. Sandfeld, Z. Budrikis, S. Zapperi, D. Fernandez Castellanos, Avalanches, loading and finite size effects in 2d amorphous plasticity: results from a finite element model, *Journal of Statistical Mechanics: Theory and Experiment* 2015 (2) (2015) 02011.
- [50] K. Karimi, J.-L. Barrat, Role of inertia in the rheology of amorphous systems: A finite-element-based elastoplastic model, *Physical Review E* 93 (2) (2016) 022904. doi:10.1103/PhysRevE.93.022904.
- [51] M. Lerbinger, A. Barbot, D. Vandembroucq, S. Patinet, Relevance of shear transformations in the relaxation of supercooled liquids, *Phys. Rev. Lett.* 129 (2022) 195501. doi:10.1103/PhysRevLett.129.195501.
- [52] J. A. Zimmerman, D. J. Bammann, H. Gao, Deformation gradients for continuum mechanical analysis of atomistic simulations, *International Journal of Solids and Structures* 46 (2) (2009) 238–253.
- [53] B. Tyukodi, S. Patinet, S. Roux, D. Vandembroucq, From depinning transition to plastic yielding of amorphous media: A soft-modes perspective, *Physical Review E* 93 (6) (2016).
- [54] S. Karmakar, E. Lerner, I. Procaccia, Statistical physics of the yielding transition in amorphous solids, *Phys. Rev. E* 82 (2010) 055103.
- [55] J. Lin, E. Lerner, A. Rosso, M. Wyart, Scaling description of the yielding transition in soft amorphous solids at zero temperature, *Proceedings of the National Academy of Sciences* 111 (40) (2014) 14382–14387. arXiv:https://www.pnas.org/doi/pdf/10.1073/pnas.1406391111.
- [56] B. Tyukodi, D. Vandembroucq, C. E. Maloney, Avalanches, thresholds, and diffusion in mesoscale amorphous plasticity, *Physical Review E* 100 (4) (2019).
- [57] E. E. Ferrero, E. A. Jagla, Criticality in elastoplastic models of amorphous solids with stress-dependent yielding rates, *Soft Matter* 15 (2019) 9041–9055.
- [58] H. G. E. Hentschel, P. K. Jaiswal, I. Procaccia, S. Sastry, Stochastic approach to plasticity and yield in amorphous solids, *Phys. Rev. E* 92 (2015) 062302.
- [59] E. Lerner, I. Procaccia, C. Rainone, M. Singh, Protocol dependence of plasticity in ultrastable amorphous solids, *Phys. Rev. E* 98 (2018) 063001.
- [60] B. Shang, P. Guan, J.-L. Barrat, Elastic avalanches reveal marginal behavior in amorphous solids, *Proceedings of the National Academy of Sciences* 117 (1) (2020) 86–92. doi:10.1073/pnas.1915070117.
- [61] M. Tsamados, A. Tanguy, C. Goldenberg, J.-L. Barrat, Local elasticity map and plasticity in a model lennard-jones glass, *Phys. Rev. E* 80 (2009) 026112. doi:10.1103/PhysRevE.80.026112.
- [62] A. Nicolas, F. Puosi, H. Mizuno, J.-L. Barrat, Elastic consequences of a single plastic event: Towards a realistic account of structural disorder and shear wave propagation in models of flowing amorphous solids, *Journal of the Mechanics and Physics of Solids* 78 (2015) 333. doi:10.1016/j.jmps.2015.02.017.
- [63] A. Nicolas, K. Martens, L. Bocquet, J.-L. Barrat, Universal and non-universal features in coarse-grained models of flow in disordered solids, *Soft Matter* 10 (2014) 4648. doi:10.1039/c4sm00395k.

- [64] C. Rainone, E. Bouchbinder, E. Lerner, Pinching a glass reveals key properties of its soft spots, *Proceedings of the National Academy of Sciences* 117 (10) (2020) 5228. doi:10.1073/pnas.1919958117.
- [65] J. E. Sinclair, P. C. Gehlen, R. G. Hoagland, J. P. Hirth, Flexible boundary conditions and nonlinear geometric effects in atomic dislocation modeling, *Journal of Applied Physics* 49 (7) (1978) 3890. doi:10.1063/1.325395.
- [66] D. Ruan, S. Patinet, M. L. Falk, Predicting plastic events and quantifying the local yield surface in 3D model glasses, *Journal of the Mechanics and Physics of Solids* 158 (2022) 104671.

## Appendix A. Evolution of stress fluctuations

The macroscopic stress fluctuations are computed as a function of the applied strain. The comparison is made between the atomic simulations and the calibrated elasto-plastic model, taking into account the memory effect through the nonlinear relation Eq. 4.1.

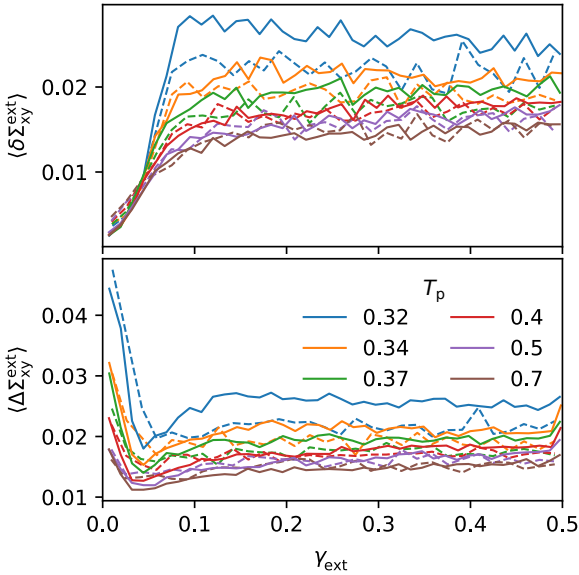


Figure A.8: External stress drops (top) and increments (bottom) vs. applied strain, for different parent temperatures  $T_p$ . The continuous lines correspond to the elasto-plastic model and the dashed lines to the atomistic one.

The fluctuations are quantified through the variations of stress increments  $\Delta\Sigma_{\text{ext}}^{\text{xy}}$  and stress drops  $\delta\Sigma_{\text{ext}}^{\text{xy}}$  as reported in Fig. A.8. The drops (increments) of macroscopic stresses increase (decrease) during the pseudo-elastic regime to quickly stabilize around a plateau, slowly converging to a steady state. A good agreement is obtained between the elasto-plastic model and atomistic simulations. However, a deviation is observed for the most stable glasses obtained from  $T_p = 0.32$  for which the increments and drops are slightly greater than atomistic simulations. The two effects nevertheless compensate each other, thus giving an average of the macroscopic stresses in good agreement with the microscopic model as shown in Fig. 1. Since this discrepancy is observed only for the most stable glass and after the peak stress, it is presumably related

to shear banding and strain localization where the small strain framework of the elastoplastic model ceases to be valid.

## Appendix B. Fitting procedure

The stationary state parameters are known from [1], except for the value of  $\chi$ . This change is due to the law  $\gamma_{\text{max}}(\tau^c)$  in Eq. 3.5 that is used in this work, in contrast with the law  $\gamma_{\text{max}}(\tau)$  of [1]. The stationary state parameters are given in Tab. B.1.

The values of  $G_q$  are measured from the quenched effective elastic response of the atomistic samples. The value of  $\text{std}[\text{dev}(\epsilon_{\text{pl}}^0)]$  is calibrated from the quenched state average von Mises stress  $\tilde{\Sigma}_{\text{vm}}$ . The value of  $\lambda_q$  and  $k_q$  are calibrated from the quenched state average local yield stress  $\langle\tilde{\tau}^c\rangle$  and the standard deviation  $\text{std}(\tilde{\tau}^c)$ . These local quantities are measured using the biggest patch size available, i.e.,  $R = 30$ . The quenched state parameters are given in Tab. B.2.

Finally, the transient parameters  $\bar{\gamma}_t$  and  $\beta$  were calibrated by using the stationary and quenched state calibrations. In this case, a global fit to all the stress-strain curves corresponding to different parent temperatures  $T_p$  was performed. These parameters are reported in Tab. B.3.

$\lambda_s$	2.05
$k_s$	2.18
$\chi$	1.81
$G_s$	13.2
$B_s$	59.0

Table B.1: Stationary state parameters.

$T_p$	$\text{std}[\text{dev}(\epsilon_{\text{pl}}^0)]$	$G_q$	$\lambda_q$	$k_q$
0.32	0.012	17.6	2.47	3.42
0.34	0.012	15.6	1.97	3.49
0.37	0.013	14.5	1.53	4.09
0.40	0.014	13.0	1.30	4.20
0.50	0.015	11.7	1.14	4.39
0.70	0.015	10.9	0.94	5.40

Table B.2: Quenched state parameters.

$\bar{\gamma}_t$	0.2
$\beta$	-3.3

Table B.3: Transient regime parameters.